Surrogate-assisted robust design optimization and global sensitivity analysis of a directly coupled photovoltaic-electrolyzer system under techno-economic uncertainty[☆]

Diederik Coppitters[a,b,c,*], Ward De Paepe[c], Francesco Contino[a,b]

[a] *Fluid and Thermal Dynamics (FLOW), Vrije Universiteit Brussel, Pleinlaan 2, 1050 Brussels, Belgium*
[b] *Combustion and Robust Optimization Group (BURN),Vrije Universiteit Brussel (VUB) and Université Libre de Bruxelles (ULB), 1050 Brussels, Belgium*
[c] *Thermal Engineering and Combustion Unit, University of Mons (UMONS), Place du parc 20, 7000 Mons, Belgium*

Abstract

To match intermittent solar energy supply with energy demand, power-to-hydrogen is a viable solution. In this framework, designing a directly coupled photovoltaic-electrolyzer system assuming deterministic parameters (i.e. perfectly known and fixed parameters) is widely studied. However, considering deterministic model parameters in optimization disregards the inherent uncertainty of the system performance during real-life operation (e.g. due to unexpected costs or ineffective maintenance), leading to a fragile, suboptimal direct coupling of the photovoltaic array with the electrolyzer stack. To avoid a suboptimal coupling, we performed a design optimization under parameter uncertainties (i.e. robust design optimization). This paper provides the deterministic designs, robust designs and a global sensitivity analysis on the hydrogen production and levelized cost of hydrogen. The technical robust design provides a 43 % reduction in hydrogen production standard deviation compared to the deterministic design, while the robust, cost-efficient design achieves a mean lev-

[☆] The short version of the paper was presented at ICAE2018, Aug 22-25, Hong Kong. This paper is a substantial extension of the short version of the conference paper.

[*] Corresponding author
Email address: dcoppitt@vub.be (Diederik Coppitters)

elized cost of hydrogen of 6.4 €/kg and standard deviation of 0.74 €/kg. The discount rate and capital expenditure parameters dominate the standard deviation by 52 % and 39 % respectively. Therefore, bulk manufacturing of these technologies and more demonstration projects are the main actions to improve the robustness. Future works will focus on including accurate probability distributions, a demand load, the grid and batteries to the system.

Keywords: `Photovoltaic-electrolyzer system, levelized cost of hydrogen, robust design optimization, uncertainty quantification, global sensitivity analysis.`

---

1. Introduction

The Sun provides around 5×10^{22} J of harvestable energy annually, which exceeds the global energy demand by several orders of magnitude [1]. Despite the large solar energy capacity available, the Sun is an intermittent energy resource, which results in a mismatch between solar energy supply (e.g. PhotoVoltaic (PV) array) and user demand. To match the supply and demand, the PV technology can be coupled with an energy storage system. Battery energy storage is the most widespread storage technology, with a round-trip efficiency ranging between 60 % and 80 % [2]. Due to this high efficiency, batteries are suitable for fast response in intermittent grid balancing. However, during longer storage periods (e.g. weeks, months), battery storage suffers from a high energy leakage (1 % - 5 % per hour) and low energy density compared to hydrogen-based energy storage [3]. Consequently, hydrogen provides a viable alternative as an energy carrier for long-term solar energy storage [2]. Among different renewable hydrogen production methods, water electrolysis is the most developed and provides high-purity hydrogen [4]. Despite being more expensive than the conventional fossil-based hydrogen production methods (e.g. around 2 €/$\mathrm{kg_{H_2}}$ for steam reforming, as opposed to 6 €/$\mathrm{kg_{H_2}}$ for photovoltaic electrolysis [5]), the water footprint is comparable (e.g. 18 $\mathrm{kg_{H_2O}/kg_{H_2}}$ for electrolysis, 22 $\mathrm{kg_{H_2O}/kg_{H_2}}$ for

Nomenclature

LCOH	Levelized Cost Of Hydrogen, €/kg
A_{m}	membrane area, cm^2
CAPEX	specific capital expenditure, €/kW
CRF	Capital Recovery Factor
d	stochastic space dimension
DDO	Deterministic Design Optimization
E_{exc}	activation energy electrode reaction, J/mol
E_{pro}	activation energy proton transport, J/mol
F	Faraday constant, 96485 C/mol
G	solar irradiance, $\mathrm{W/m}^2$
i	current density, $\mathrm{A/cm}^2$
I_0	diode current, A
I_{L}	photocurrent, A
I_{PV}	PV cell current, A
I_{SC}	short-circuit current, A
k	Boltzmann constant, 1.381×10^{-23} J/K
$\dot{m}$	mass flow rate, kg/s
n	lifetime, y
n_{d}	diode ideality factor, 1.2
n_{gen}	number of generations
N_{p}	number of electrolyzers in parallel
n_{pop}	population sample size
$N_{\mathrm{PV,s}}$	number of cells in series on a photovoltaic panel
N_{s}	number of electrolyzers in series
OPEX	specific operational expenditure, €/kW
p	polynomial order
q	electron charge, 1.602×10^{-19} C
R	gas constant, 8.134 J/(mol K)
r	discount rate
RDO	Robust Design Optimization
R_{s}	series resistance, Ω
S	Sobol' index
T	temperature, K
t_{m}	membrane thickness, cm
U	voltage, V
u	PCE coefficient
U_{act}	activation overpotential, V
U_{diff}	diffusion overpotential, V
$U_{\mathrm{electrodes}}$	overpotential electrodes, V
U_{OC}	open circuit voltage, V
U_{ohmic}	ohmic voltage, V
U_{PV}	PV cell voltage, V
U_q	band gap voltage, V
U_{rev}	reversible potential, V
X_U	reactance, Ω
z	coefficient transferred electrons, 2
α	charge transfer coefficient
η	efficiency
μ	mean
σ	standard deviation
σ_{m}	membrane conductivity, Sv/cm
Ψ	orthogonal polynomial
a	anode
amb	ambient
c	cathode
elec	electrolyzer

steam methane reforming [6]). In the framework of solar-powered water electrolysis, the direct coupling of PV energy systems with electrolyzers is widely studied [3, 7, 8]. When considering direct coupling, the inclusion of DC-DC converters with Maximum Power Point (MPP) tracking is avoided, which reduces the system complexity, cost and transmission loss. As a result, this approach results in the highest economic performance for low power applications [7].

When designing a directly coupled PV-electrolyzer system, multiple objectives can be defined to determine the system performance. In Khalilnejad et al. [3], a hybrid PV and wind turbine system is coupled with a 10 kW electrolyzer. In this work, the system is designed such that the system excess power production, divided by the hydrogen production, is minimized. In Maroufmashat et al. [7], the electrolyzer stack is designed to minimize the annual energy loss and maximize the hydrogen production. In García-Valverde et al. [8], the number of electrolyzers in series is defined to maximize the energy transfer from 72 series-connected solar panels. From previous work, it is clear that the hydrogen production and energy loss are common PV-electrolyzer system objectives. While the hydrogen production is a technical performance indicator, the energy transfer loss is only an indirect economic performance indicator. Instead, the Levelized Cost Of Hydrogen (LCOH) is generally used to indicate the techno-economic performance of hydrogen-based energy systems [9]. In a recent work of Sayedin et al. [10], a first techno-economic design optimization of a directly coupled PV-electrolyzer system is performed, aiming to minimize the energy transfer loss and LCOH by configuring the number of electrolyzers in series and parallel. Despite its clear significance (cost estimated around 11 €/kWh [11]), the hydrogen storage system is rarely addressed in directly coupled PV-electrolyzer optimization studies, as these studies focus on the feasibility of producing renewable hydrogen in this way. Moreover, water treatment (energy consumption ranging between 1.5 kW h/m^3 and 2.5 kW h/m^3, cost ranging between 0.40 €/m^3 and 1.52 €/m^3 [12]) and potential oxygen revenues (59 €/Nm^3 for medical grade oxygen from retail level vendors, 0.069 €/Nm^3 for large industrial scale producers [13]) are not addressed.

In previous design optimization strategies, the model parameters are considered deterministic. Any deviation from these deterministic parameter values during real-life operation can lead to suboptimal coupling and performance of the PV-electrolyzer system. Therefore, the uncertainty on the system parameters is characterized by probability density functions. To quantify the effect of the input parameter uncertainty on the system objectives (i.e. Uncertainty Quantification (UQ)), Monte Carlo Simulation is a robust, easy-to-implement technique that provides accurate statistical moments (e.g. mean, standard deviation) on the objective, at the expense of a large number of model evaluations ($\approx 10^4$) [14]. While this low computational efficiency is irrelevant for linear, fastly-evaluated system models, applying Monte Carlo Simulation becomes computationally intractable on a non-linear model subject to a significant evaluation time. To improve the computational efficiency, surrogate models such as Polynomial Chaos Expansion (PCE) are widely used to propagate the uncertainties in more complex system models [14–16]. To create a PCE surrogate model, the number of model evaluations required is based on the number of considered uncertain parameters (i.e. stochastic dimension) and the model complexity. To illustrate: considering 10 uncertain model parameters where the relation between inputs and objective can be approximated by multivariate orthogonal polynomials of order 3, PCE requires 572 model evaluations to provide accurate statistical moments on the objective. When the surrogate model is constructed, the statistical moments of the objective follow analytically [16].

To find a set of system designs that make a trade-off between optimizing the objective mean and minimizing the standard deviation, we coupled PCE with a multi-objective optimization algorithm. The design leading to the minimum standard deviation is least sensitive to the model parameter uncertainties and therefore ensures the highest quality of the system outcome during real-life operation. This approach is defined as surrogate-assisted Robust Design Optimization (RDO) [15] and represents one of the strategies out of the robust optimization spectrum. In this spectrum, another established approach is the methodology of Taguchi [17], where several designs are evaluated under varying

noise factors (e.g. environmental conditions, manufacturing tolerances), whereafter the design leading to the minimum mean square deviation is considered as the robust design. Alternatively, during worst case scenario-based design optimization, the loss in objective function is minimized by designing the system assuming the least favourable conditions (i.e. min-max optimization) [18]. To address the over conservativeness of this method, a different approach was presented, where the degree of conservativeness can be controlled by the user [19]. RDO is applied in various domains, including fatigue analysis and structural dynamics [15]. In energy systems, the application of RDO is limited to linear models, a single economic objective, a limited number of uncertain parameters based on expert judgement and an assumption on the uncertainty range [20–23]. To illustrate, in Akbari et al. [23], a robust design of a distributed energy system is investigated, where a 20 % range is applied to a handful of demand and financial parameters.

The characteristics of a techno-economic robust design of a directly coupled PV-electrolyzer system are not yet demonstrated. Next to that, the operating temperature is rarely considered as a design parameter and no specific techno-economic uncertainties are applied. As the optimality of the direct coupling strongly depends on the electrolyzer stack configuration and therefore on the assumed techno-economic parameter values, we applied a surrogate-assisted RDO for various climate conditions to ensure an optimal, robust direct coupling of the PV-electrolyzer system. Next to the number of electrolyzers in series and parallel, which are common design parameters in literature, the operating temperature is selected as an additional design parameter. All technical and economic model parameters are considered uncertain and the ranges are based on literature rather than using a general assumption. Thereafter, a stochastic dimension reduction is applied to determine the parameters that contribute significantly to the objective variation, instead of relying on the vaguely defined modeller judgement. When the robust designs are characterized, their advantages are illustrated compared to the respective deterministic designs. For each robust design, the individual contribution of each uncertain parameter to the

objective variation is quantified. The determination of these individual contributions allows the formulation of technical and economic guidelines to further enhance the robustness of the performance during real-life operation. In this paper, first the PV-electrolyzer system model and the optimization procedures are described in section 2. In section 3, the results of the deterministic optimal designs and the robust design performance are discussed, followed by the conclusions in section 4.

2. System modelling and optimization procedures

In this section, the system models and climate data are presented, followed by the optimization parameters and algorithm. To determine the robust design and its performance, the uncertainty characterization, UQ and surrogate-assisted RDO methods are discussed. The considered system models and algorithms are developed in Python.

2.1. System model

The adopted models for the PV system and the electrolyzer stack are described, followed by the climate data of the three locations considered in this study.

2.1.1. Photovoltaic system array

To convert the solar energy into electric power, we take a PV array of 72 series-connected MSX-60 panels [8, 24]. A single PV cell is characterized based on a single diode model without parallel resistance, following the experimentally validated structure presented by González-Longatt [25].

The produced PV cell current I_{PV} depends on the photocurrent I_{L}, the diode current I_0 and the series resistance R_{s}:

$$I_{\mathrm{PV}} = I_{\mathrm{L}} - I_0 \left(\exp\left(\frac{q(U_{\mathrm{PV}} + I_{\mathrm{PV}} R_{\mathrm{s}})}{n_{\mathrm{d}} k T_{\mathrm{amb}}} \right) - 1 \right), \tag{1}$$

where q is the electron charge, n_{d} the diode ideality factor and k the Boltzmann constant. To solve this non-linear equation for I_{PV}, we used the Newton-Raphson numerical method for its fast convergence and accuracy [25, 26]. The

photocurrent I_{L} depends on the solar irradiance G and ambient temperature T_{amb}:

$$I_{\mathrm{L}} = I_{\mathrm{SC}}(T_{1,\mathrm{nom}})\frac{G}{1000} + K_0(T_{\mathrm{amb}} - T_1). \tag{2}$$

The coefficient K_0 depends on 2 reference temperatures and the corresponding short-circuit currents I_{SC}:

$$K_0 = \frac{I_{\mathrm{SC}}(T_2) - I_{\mathrm{SC}}(T_1)}{T_2 - T_1}. \tag{3}$$

The diode current I_0 is represented according to the following equation:

$$I_0 = I_0(T_1)\left(\frac{T_{\mathrm{amb}}}{T_1}\right)^{\frac{3}{n}} \exp\left(\frac{qU_q(T_1)}{nk\left(\frac{1}{T_{\mathrm{amb}}} - \frac{1}{T_1}\right)}\right), \tag{4}$$

where $I_0(T_1)$ is given by:

$$I_0(T_1) = \frac{I_{\mathrm{SC}}(T_1)}{\left(\exp\left(\frac{qU_{\mathrm{OC}}(T_1)}{nkT_1}\right) - 1\right)}. \tag{5}$$

The series resistance represents the internal losses:

$$R_{\mathrm{s}} = -\frac{\mathrm{d}U}{\mathrm{d}I_{U_{\mathrm{OC}}}} - \frac{1}{X_U}, \tag{6}$$

where the term $\mathrm{d}U/\mathrm{d}I_{U_{\mathrm{OC}}}$ is equal to $1.15/2/N_{\mathrm{PV,s}}$, based on the PV panel current-voltage characteristic provided by the manufacturer [25]. X_U is given by:

$$X_U = I_0(T_1)\frac{q}{nkT_1} \exp\left(\frac{qU_{\mathrm{OC}}(T_1)}{nkT_1}\right) - \frac{1}{X_U}. \tag{7}$$

The shunt resistance, which corresponds to the leakage current to the ground, is commonly neglected and therefore it is not considered in this work [25, 27].

2.1.2. Electrolyzer stack

To produce hydrogen from an intermittent electricity supply, we selected a Proton Exchange Membrane (PEM) electrolyzer, based on its fast response time (<1 s) and full operational flexibility [28]. The electrolyzer operates at

atmospheric pressure, as the coupling of pressurized electrolyzers with intermittent energy sources is less robust, due to problems such as worse cross-permeation phenomena, corrosion, hydrogen embrittlement [29] and smaller operating range [30] as opposed to atmospheric pressure electrolysis. To characterize the PEM electrolyzer, we adopted the experimentally validated model of Garcia-Valverde et al. [29]. To induce an electric current in the PEM electrolyzer, an operating voltage U_{elec} has to be applied:

$$U_{\mathrm{elec}} = U_{\mathrm{rev}} + U_{\mathrm{electrodes}} + U_{\mathrm{ohm}}. \tag{8}$$

U_{rev} is reversible potential, $U_{\mathrm{electrodes}}$ the overpotential at the electrodes and U_{ohm} the ohmic overpotential. At atmospheric pressure, the reversible potential U_{rev} is found empirically:

$$U_{\mathrm{rev}} = 1.5184 - 1.5421\ 10^{-3} T_{\mathrm{elec}} + 9.523\ 10^{-5} T_{\mathrm{elec}} \ln T_{\mathrm{elec}} + 9.84\ 10^{-8} T_{\mathrm{elec}}^2. \tag{9}$$

While the reversible potential represents only the open circuit voltage, an overpotential has to be applied to induce the electric charge transfer and to overcome the mass transport phenomena. This required overpotential is represented by the activation overpotential and diffusion overpotential respectively:

$$U_{\mathrm{electrodes}} = U_{\mathrm{act}} + U_{\mathrm{diff}}. \tag{10}$$

However, the mass transport phenomena are relatively small at low current densities [29]. Therefore, this effect is negligible in commercial PEM electrolysers and is not considered in this work. The activation overpotential is defined by the overpotential that is distributed over the anode and cathode, where respectively the reduction and oxidation take place:

$$U_{\mathrm{act}} = U_{\mathrm{act,a}} + |U_{\mathrm{act,c}}|, \tag{11}$$

$$U_{\mathrm{act,a}} = \frac{R T_{\mathrm{elec}}}{\alpha_{\mathrm{a}} z F} \ln\left(\frac{i_{\mathrm{a}}}{i_{0,\mathrm{a}}}\right), \tag{12}$$

$$U_{\mathrm{act,c}} = \frac{R T_{\mathrm{elec}}}{\alpha_{\mathrm{c}} z F} \ln\left(\frac{i_{\mathrm{c}}}{i_{0,\mathrm{c}}}\right). \tag{13}$$

The activation overpotential depends on the ideal gas constant R, the operating temperature of the electrolyzer T_{elec}, the coefficient of transferred electrons z (= 2 for water electrolysis), the Faraday constant F (= 96 485 C/mol) and the current density i. The electrode contribution to the overpotential is unequally divided. The anode exchange current density is generally much lower ($\approx 10^{-7}$ A/cm^2) than at the cathode electrode ($\approx 10^{-3}$ A/cm^2) [29]. Therefore, we neglected the cathode contribution. By using the common assumption of a symmetric reaction, the charge transfer coefficients α are equal to 0.5. To define the exchange current density, an Arrhenius expression is applied, which characterizes the effect of the operating temperature on the current density:

$$i_0 = i_{0,\mathrm{ref}} \exp\left(-\frac{E_{\mathrm{exc}}}{R}\left(\frac{1}{T_{\mathrm{elec}}} - \frac{1}{T_{\mathrm{ref}}}\right)\right). \tag{14}$$

Where E_{exc} is the activation energy for the electrode reaction. The final overpotential that defines the operating voltage is the Ohmic overpotential, which depends on the resistive losses:

$$U_{\mathrm{ohm}} = iR_{\mathrm{l}} = i(R_{\mathrm{ele}} + R_{\mathrm{ion}}). \tag{15}$$

The electronic contribution to the resistive losses is limited compared to the ionic contribution, since the membrane conductivity is significantly lower than the conductivity in the other components [29]. The ionic membrane resistance depends on the thickness and conductivity:

$$R_{\mathrm{ion}} = \frac{t_{\mathrm{m}}}{\sigma_{\mathrm{m}}}. \tag{16}$$

Assuming a fully hydrated membrane, the membrane conductivity can be modelled using an Arrhenius expression at a reference temperature:

$$\sigma_{\mathrm{m}} = \sigma_{\mathrm{m,ref}} \exp\left(-\frac{E_{\mathrm{pro}}}{R}\left(\frac{1}{T_{\mathrm{ref}}} - \frac{1}{T_{\mathrm{elec}}}\right)\right), \tag{17}$$

where E_{pro} is the activation energy for the proton transport in the membrane. When combining the electrolyzers in parallel N_{p} and series N_{s}, the electrolyzer stack voltage and current are expressed as:

$$U_{\mathrm{stack}} = N_{\mathrm{s}} U_{\mathrm{elec}}, \tag{18}$$

$$I_{\text{stack}} = N_{\text{p}} I_{\text{elec}}. \tag{19}$$

The hydrogen production is proportional to the current:

$$\dot{m}_{\text{H}_2} = \frac{N_{\text{s}} I_{\text{stack}}}{2000F} \eta_{\text{F}}, \tag{20}$$

where η_{F} is the Faraday efficiency that represents the loss in hydrogen collection due to leakage and electrons that do not participate in the decomposition reaction [31].

2.1.3. Climate data

To analyze the effect of different climate conditions on the system, we considered hourly solar irradiance and ambient temperature data for one year for Bern in Switzerland (46.9 °N, 7.4 °E), San Francisco in the United States of America (37.8 °N, −122.5 °E) and Johannesburg in South-Africa (−26.2 °N, 28.0 °E) [32]. Clearly, these locations are subject to different climate conditions, where Johannesburg achieves the highest total yearly solar irradiance and average yearly ambient temperature, followed by San Francisco and Bern (Table 1). Due to the variability in the climate conditions, the PV system in each location produces different PV system characteristics and MPPs over the year. The MPPs in Johannesburg are concentrated in the top-right region of the current-voltage graph, resulting in the highest yearly power production, while in the other locations the MPPs are more widespread (Figure 1).

Table 1: The climate data for the considered locations illustrate that Johannesburg receives the highest total yearly solar irradiance and highest average ambient temperature.

Location	G_{total}	μ_G	σ_G	$\mu_{T_{\text{amb}}}$	$\sigma_{T_{\text{amb}}}$
	kWh/m^2/year	W/m^2	W/m^2	°C	°C
Bern	1243	143	262	10.7	8.0
San Francisco	1842	210	303	14.2	4.1
Johannesburg	2302	263	373	16.0	5.8

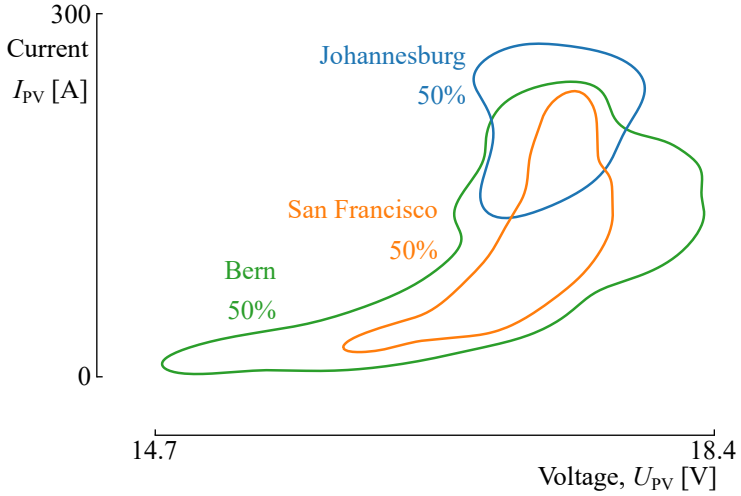

Figure 1: To illustrate the effect of the variability of the climate conditions, the region is marked where 50 % of the hourly produced Maximum Power Points (MPPs) over the year are situated. Clearly, during the year, the climate conditions in Johannesburg induce that 50 % of the MPPs produced by the PV array are located in the high-current, high-voltage region. The MPPs produced in San Francisco and Bern are more widespread towards lower currents and voltages, resulting in a lower overall power production during the year.

2.2. Deterministic Design Optimization

In this section, the design parameters and objectives are defined for the PV-electrolyzer system, as well as the optimization algorithm.

2.2.1. Design parameters and objective

The solar irradiance is converted into electrical energy by the PV array. To convert the electrical energy into hydrogen, an electrolyzer stack is directly coupled to the PV array. Due to this direct coupling, the electrolyzer stack needs to be configured such that the optimal energy transfer occurs from the PV panels to the electrolyzer stack. To find an optimal configuration for the electrolyzer stack for each considered location, the number of electrolyzers in series [7], the number of parallel strings of series electrolyzers [7] and the operating temperature [28] are selected as design parameters:

$$1 \leq N_{\mathrm{s}} \leq 30,$$

$$1 \leq N_{\mathrm{p}} \leq 30,$$

$$323 \text{ K} \leq T_{\mathrm{elec}} \leq 353 \text{ K}. \tag{21}$$

By adapting these design parameters, the electrolyzer stack characteristic is modified, resulting in a different intersection point for the PV system characteristic and electrolyzer stack characteristic and therefore a change in transferred power between both systems (Figure 2). To illustrate, increasing the operating temperature decreases the operating voltage for the same current density. Therefore, less electrical power is required for the same current flowing through the stack. At a higher operating temperature, the electrochemical reaction rate is improved, resulting in higher exchange current density and decreased voltage loss [33].

To characterize the PV-electrolyzer system techno-economic performance for each design sample, the LCOH is quantified. The LCOH depends on the hydrogen production, CAPEX and OPEX of the installed PV panels and electrolyzers [34]:

$$\mathrm{LCOH} = \frac{\mathrm{CRF}(\mathrm{CAPEX}_{\mathrm{PV}} + \mathrm{CAPEX}_{\mathrm{elec}}) + \mathrm{OPEX}_{\mathrm{PV}} + \mathrm{OPEX}_{\mathrm{elec}}}{\sum_{i=1}^{8760} \dot{m}_{\mathrm{H_2},i}}, \tag{22}$$

where CRF is the Capital Recovery Factor, which is characterized by the discount rate r and system lifetime n:

$$\mathrm{CRF} = \frac{(r(1+r)^n)}{(1+r)^n - 1}. \tag{23}$$

The considered values for the different parameters are listed in Table 2.

2.2.2. Optimization algorithm

Based on the complexity and non-linearity of the system, we implemented the Nondominated Sorting Genetic Algorithm (NSGA-II) to find the set of optimal design samples [35, 36]. This set corresponds to the design samples that dominate every other sample in at least one objective (i.e. Pareto set of design

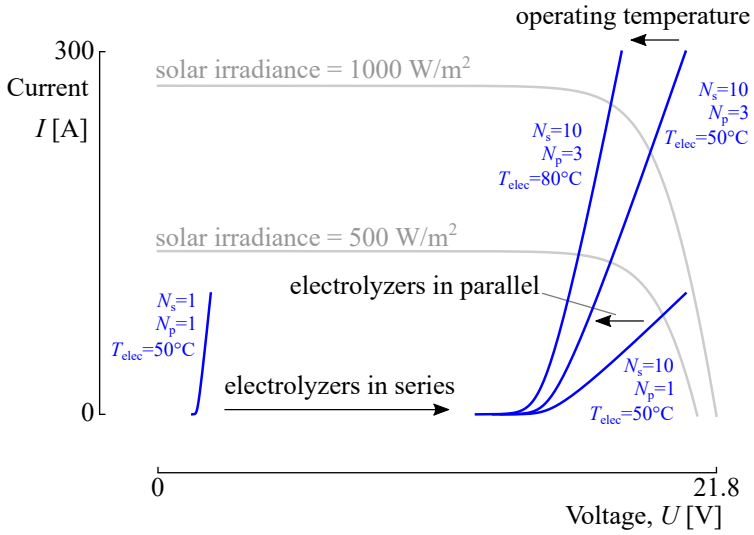

Figure 2: The voltage and current transferred from the PhotoVoltaic (PV) array to the electrolyzer stack is defined at the intersection point of the PV and electrolyzer stack voltage-current characteristic. The electrolyzer stack characteristic can be adapted by changing the stack configuration: The operating voltage is proportional to the number of electrolyzers in series (N_{s}), while adding electrolyzers in parallel (N_{p}) increases the limiting current of the electrolyzer stack and therefore the range of the characteristic. Finally, the stack characteristic is steepened by increasing the number of electrolyzers in parallel and increasing the operating temperature (T_{elec}).

samples). The metaheuristic NSGA-II algorithm starts from an initial set of design samples (i.e. population), which is configured based on Latin Hypercube Sampling [37]. Out of these initial samples, offsprings are created based on crossover and mutation rules, which are represented by the evaluated binary bounded [38] and polynomially bounded [39] operators respectively. The initial population samples and offspring samples are evaluated in the PV-electrolyzer model and sorted based on their dominance in the objectives. Moreover, when no mutual domination occurs between samples, the most isolated samples in the design space are favoured over samples in more crowded regions. As a result, the diversification of the final solution set will be improved. This process is repeated until convergence is reached, or when the predefined maximum number

of iterations (i.e. generations) is reached. In this work, the population n_{pop} is set at 24 design samples, while the optimization algorithm is configured with a crossover and mutation probability of 0.9 and 0.1 respectively. The population samples are evaluated in parallel on a 12 core Intel®Xeon®CPU E5-2687W v4 3.00 GHz. To illustrate, with a single model evaluation taking around 6 s, running the Deterministic Design Optimization (DDO) over 250 generations takes around 1 hour.

2.3. Surrogate-assisted Robust Design Optimization

In the previous section, the design optimization has been illustrated assuming deterministic parameters (i.e. free from inherent variation). In this section, the uncertainty on the parameters is introduced. First, the uncertainty characterization of the techno-economic parameters is described, followed by the UQ technique to define the effect of uncertain input parameters on the objective. To reduce the computational cost of the surrogate-assisted RDO, the stochastic dimension reduction technique is introduced. The section concludes with the surrogate-assisted RDO algorithm.

2.3.1. Uncertainty characterization

While in DDO all the parameters are considered deterministic, in real-life these parameters are subject to uncertainties. To represent real-world conditions, in this section, the technical and economic parameters of the PV-electrolyzer system are characterized as uncertain (Table 2). For the system economics, the CAPEX and OPEX are considered uncertain. While the design optimization on system models employs at an early stage to evaluate the feasibility, the final investment stage usually occurs at a significantly later time, as it is preceded by a thorough planning study. Therefore, the proposed designs are vulnerable to changing market conditions, leading to uncertainty in the initial investment cost. Next to that, the OPEX can be considered uncertain, as unexpected operating costs might emerge. Next, considering uncertainty on the discount rate takes into account changes in finance types and policies [40]. The

technical parameters of the PV-electrolyzer system are subject to commissioning and maintenance quality during operation. Moreover, inherent parameter variations are present, as well as measurement inaccuracy [40]. The limiting current i_{lim}, which forms a constraint on the operating range of the electrolyzer, is considered at its worst-case value. This will ensure, with a reliability of 3 times the standard deviation, that the proposed design will not violate the constraint due to the uncertain behaviour of the model parameters. The climate data (e.g. solar irradiance and ambient temperature) can be considered uncertain due to measurement inaccuracy, inter-annual variability and spatial variability [40]. In this work, all uncertainties follow a Gaussian distribution.

2.3.2. Uncertainty Quantification

As the model input parameters are considered uncertain, these uncertainties will propagate through the PV-electrolyzer system model and affect the objective quantification. Consequently, the objective is no longer characterized by a deterministic value, but by a probability density function instead, which is characterized by statistical moments (e.g. mean, standard deviation). To quantify the statistical moments of the objective, an UQ technique is required. While Monte Carlo Simulation is a robust technique (i.e. always reaching convergence), it has a low computational efficiency ($\approx 10^4$ model evaluations required to reach an acceptable accuracy on the objective statistics) [14]. In this work, we applied PCE instead to quantify the objective statistical moments efficiently [14, 16].

The PCE surrogate model $\hat{M}(\boldsymbol{\xi})$ of the physical model $M(\boldsymbol{\xi})$ is represented as:

$$\hat{M}(\boldsymbol{\xi}) = \sum_{i=0}^{P} u_i \Psi_i(\boldsymbol{\xi}) \approx M(\boldsymbol{\xi}). \tag{24}$$

In this equation, Ψ_i represents a multivariate orthogonal polynomial, u_i is the corresponding coefficient and $\boldsymbol{\xi} = (\xi_1, \xi_2, ..., \xi_d)$ is the set of independent stochastic model parameters, with d the dimension of the stochastic design space (i.e. the number of uncertain parameters considered). The type of orthogonal polynomials are selected based on the input parameter probability distributions, in

Table 2: For the PV-electrolyzer system model, 18 techno-economic model parameters are considered uncertain. The limiting current constraint is considered at its worst-case scenario, to ensure that no constraint violation occurs due to the model parameter variations.

Parameter	Deterministic value	Range
$\mathrm{CAPEX_{PV}}$	780 €/kW [41]	± 520 €/kW [41]
$\mathrm{OPEX_{PV}}$	17.5 €/kW/y [41]	± 1.5 €/kW/y [41]
n_{PV}	25 y [41]	± 5 y [42]
$\mathrm{CAPEX_{elec}}$	1750 €/kW [28]	± 350 €/kW [28]
$\mathrm{OPEX_{elec}}$	4 % [28]	± 1 $\%_{\mathrm{abs}}$ [28]
n_{elec}	80.000 h [28]	± 20.000 h [28]
r	6 % [43]	± 4 $\%_{\mathrm{abs}}$ [44]
$\mu_{I_{\mathrm{SC}}}$	0.065 A/K [24]	± 0.015 A/K [24]
$\mu_{U_{\mathrm{OC}}}$	0.08 V/K [24]	± 0.01 V/K [24]
I_{SC}	3.8 A [24]	± 0.1 A [24]
U_{OC}	21.1 V [24]	± 0.1 V [24]
A_{m}	50 cm^2 [29]	± 1 cm^2
t_{m}	0.0051 cm [7]	± 0.0001 cm
η_{F}	99.5 % [29]	± 0.5 % [29]
U_{degr}	6 µV/h [28]	± 2 µV/h [28]
T_{elec}	design parameter	± 1 K [45]
G	hourly data for one year [32]	± 7 % [32]
T_{amb}	hourly data for one year [32]	± 0.5 K [32]
i_{lim}	2 $\mathrm{A/cm}^2$ [7]	−2 % [29]

accordance with the Askey scheme [14]. As in this work, the input parameters follow a Gaussian distribution, the Hermite orthogonal polynomial family is selected accordingly. If an infinite series of orthogonal polynomials and corresponding coefficients are considered, the PCE surrogate model is an exact representation of the initial model. However, since an infinite series is computationally intractable, a truncated series is implemented instead. This truncated

series consists of P elements, where P depends on the complexity of the initial model (related to the polynomial order p) and the number of considered uncertain parameters d:

$$P + 1 = \frac{(p+d)!}{p!d!}. \tag{25}$$

To quantify the PCE coefficients u_i, we applied a non-intrusive regression approach [16]. Out of these PCE coefficients, the mean μ and standard deviation σ follow analytically:

$$\mu = u_0 \tag{26}$$

$$\sigma^2 = \sum_{i=1}^{P} u_i^2 \tag{27}$$

For the PV-electrolyzer model, a polynomial order of 3 results in an error below 1 % on the statistical moments for the objective, compared to a Monte Carlo Simulation result of 10^5 model evaluations.

Next to the statistical moments, the Sobol' indices can be quantified analytically out of the PCE coefficients. The Sobol' indices represent the contribution of one or combined stochastic input parameters to the total variance of the objective [14]. To illustrate, the first-order Sobol' indices are defined as:

$$S_i = \frac{D_i}{D} = \frac{\mathrm{Var}[M(\xi_i)]}{\mathrm{Var}[M(\boldsymbol{\xi})]}. \tag{28}$$

The first-order Sobol' indices are found out of the PCE coefficients by a mere combination of the squares of the related coefficients to that input parameter:

$$S_i^{PC} = \sum_{\alpha \in A_i} u_\alpha / D \qquad A_i = \{\alpha \in A : \alpha_i = 0, \alpha_{j \neq i} = 0\}, \tag{29}$$

where A is the set containing all coefficients in the truncated series.

2.3.3. Stochastic dimension reduction

When considering the full stochastic design space, out of Equation 25 follows that 1330 model evaluations are required to acquire accurate statistical moments for the objectives. Moreover, to ensure an accurate quantification of the coefficients through regression, 2 to 3 times that amount of model evaluations are

required [14]. The exponential increase of model evaluations with the number of uncertain inputs in PCE is referred to as the curse-of-dimensionality [16]. Therefore, in this section, a stochastic dimension reduction [46, 47] is applied to determine the uncertain parameters with negligible contribution to the objective variation and consider them as deterministic in the RDO algorithm.

For every design sample evaluated in the PV-electrolyzer system model, the Sobol' indices S_i related to the stochastic model parameters in that design sample can be quantified. In total, d Sobol' indices are acquired, one for each stochastic model parameter. These Sobol' indices are ranked based on their value. Consequently, the parameters with a corresponding Sobol' index below a certain threshold can be discarded from the stochastic design space and therefore be considered deterministic in future evaluations.

The contribution of a specific stochastic parameter can vary in different areas of the design space. Therefore, a computational budget is fixed to do a first screening of the design space. For this screening, one population of design samples is evaluated, which is spread over the design space by Latin Hypercube Sampling [14]. This results in n_{pop} values for the Sobol' index of each stochastic parameter $\boldsymbol{S}_j = (S_{j,1}, S_{j,2}, ..., S_{j,n_{\text{pop}}})$, where $j = 1, 2, ..., d$. If $\max(\boldsymbol{S}_j) < S_{\text{thres}}$, this model parameter can be discarded from the stochastic design space and consequently be considered deterministic. In this work, a threshold S_{thres} of 2 % is selected.

2.3.4. Surrogate-assisted Robust Design Optimization algorithm

After the characterization of the uncertainty on the model parameters and the stochastic dimension reduction, the next step is to apply the surrogate-assisted RDO algorithm on the PV-electrolyzer system [15]. In the surrogate-assisted RDO algorithm, the NSGA-II algorithm is coupled with the PCE algorithm. An initial population of design samples n_{pop} is distributed over the design space and next generations are created out of the initial samples based on their dominance in the objectives (subsubsection 2.2.2). In contrast with DDO, the RDO objectives are the mean and standard deviation. Since the objectives

are the statistical moments, for each evaluated design sample a PCE surrogate model has to be created (subsubsection 2.3.2). When convergence is reached, a single optimal design is found, or a Pareto set of design samples that represents the trade-off between the optimal mean of the objective and the minimum standard deviation of the objective (i.e. optimal robustness).

3. Results and discussion

After the system modelling and the illustration of the optimization procedures, the next step is to apply the optimization algorithms on the PV-electrolyzer system model. First, the results of the DDO are presented and discussed, followed by a sensitivity analysis of the discount rate. Thereafter, the stochastic dimension reduction is applied and the surrogate-assisted RDO is performed. To conclude, a sensitivity analysis of the discount rate is performed, considering only the operational uncertainties.

3.1. Deterministic Design Optimization

In this section, the optimization algorithm is applied to find the optimal designs for the electrolyzer stack of the considered locations (i.e. Bern, San Francisco and Johannesburg), assuming deterministic parameters. While a minimum LCOH indicates an optimal techno-economic performance of the system, it does not ensure an optimal performance in terms of hydrogen production. Therefore, the hydrogen production is evaluated separately from the LCOH by the optimization algorithm, to be able to provide alternatives that aim towards a higher hydrogen production, at the expense of a larger LCOH to produce it (e.g. decentralized systems). To illustrate the effect of the discount rate on the optimal LCOH, a sensitivity analysis of the discount rate is performed.

3.1.1. Techno-economic Deterministic Design Optimization

The optimization algorithm is applied to the system, resulting in Pareto design samples that make a trade-off between minimizing the LCOH and maximizing the hydrogen production (Figure 3). The algorithm converged after 60

generations, which is comparable to the computational efficiency reported by Sayedin et al. (71 generations for a population size of 20) [48]. Despite the clear link between the power applied to the electrolyzer stack and the hydrogen production (Equation 20), a trade-off exists near the MPPs between maximizing the energy transfer efficiency from the PV array to the electrolyzer stack ($=E_{\mathrm{elec,year}}/E_{\mathrm{MPP,year}}$) and maximizing the hydrogen production (Table 3) [7]. Consequently, operating exactly in the MPP does not induce the highest hydrogen production.

For the 3 considered locations, a configuration of 2 parallel-connected strings of electrolyzers, where each string consists of 10 electrolyzers in series, results in the minimum LCOH for the system. The optimal LCOH ranges from 6.3 €/kg (Johannesburg) to 10.5 €/kg (Bern), which is comparable to recently published LCOH for directly coupled PV-electrolyzer system designs in various cities in Iran (between 7.32 €/kg and 9.46 €/kg) [10]. With 2 parallel strings of electrolyzers, the electrolyzer stack can handle up to 200 A, which is sufficient to achieve an optimal amount of operating hours for each location. To illustrate, for this configuration, in only 0.7 % of the time in Johannesburg, the produced PV power is situated outside the operating range of the electrolyzer stack. When 1 electrolyzer string in parallel is considered, this downtime is equal to 40.8 %. Next to the regulation of the limiting current of the electrolyzer stack by the number of electrolyzer strings in parallel, the operating voltage of the electrolyzer stack is mainly controlled by to the number of cells in series. Since the operating voltage range near the MPPs is narrow for all locations (Figure 1), the optimal designs in each location consist of the same number of electrolyzers in series. The final design parameter, the electrolyzer operating temperature, is slightly different: $T_{\mathrm{elec}} = 333\,\mathrm{K}$ in Johannesburg, $T_{\mathrm{elec}} = 336\,\mathrm{K}$ in San Francisco and $T_{\mathrm{elec}} = 331\,\mathrm{K}$ in Bern. Remarkably, the operating temperature in the optimal designs is selected below the highest temperature, where the minimum voltage losses would have occurred. By operating at these temperatures, the intersection points between the PV array and electrolyzer stack characteristic is optimized, resulting in the optimal hydrogen production, even if a higher oper-

ating voltage is required compared to operating at the maximum temperature. To illustrate, for this electrolyzer stack configuration, operating out of the optimal operating temperature can increase the LCOH up to 78 % in Johannesburg (Figure 4).

The PV-electrolyzer system in Johannesburg achieves the lowest LCOH out of all locations, leading thus to the highest hydrogen production, since the investment cost of the electrolyzer stack is equal in all 3 locations. Indeed, the hydrogen production ranges between 103.2 kg/year in Bern and 178.9 kg/year in Johannesburg. Therefore, the hydrogen production is proportional to the total yearly solar irradiance, while the LCOH is inversely proportional to the total yearly solar irradiance. The hydrogen production can be maximized in each location by adapting the system design into a configuration of 30 parallel-connected strings of 12 electrolyzers in series and an operating temperature of 353 K in all locations. This configuration consists of 18 times more electrolyzers than the minimum LCOH design (360 electrolyzers instead of 20), while the resulting increase in hydrogen production ranges from 30.7 % (San Francisco) to 40.9 % (Johannesburg). Consequently, the LCOH is drastically increased (≈9 times) when installing this configuration. As a trade-off between both extreme designs, an intermediate design configuration is presented, consisting of 3 parallel strings of 10 electrolyzers operating at 353 K (Table 3). This design significantly improves the hydrogen production in each location compared to the cost efficient design, at the expense of an acceptable increase in LCOH Figure 3.

3.1.2. Sensitivity analysis of the discount rate

The discount rate of the PV-electrolyzer system is a highly uncertain parameter that has a significant effect on the LCOH [44]. Therefore, in this section, the effect of the discount rate on the LCOH is quantified and the potential LCOH reduction by de-risking the technology is illustrated. For the design leading to the minimum LCOH in each location (Table 3), the discount rate is varied between 2 % and 10 %. A decrease in LCOH of 63 % is achieved in

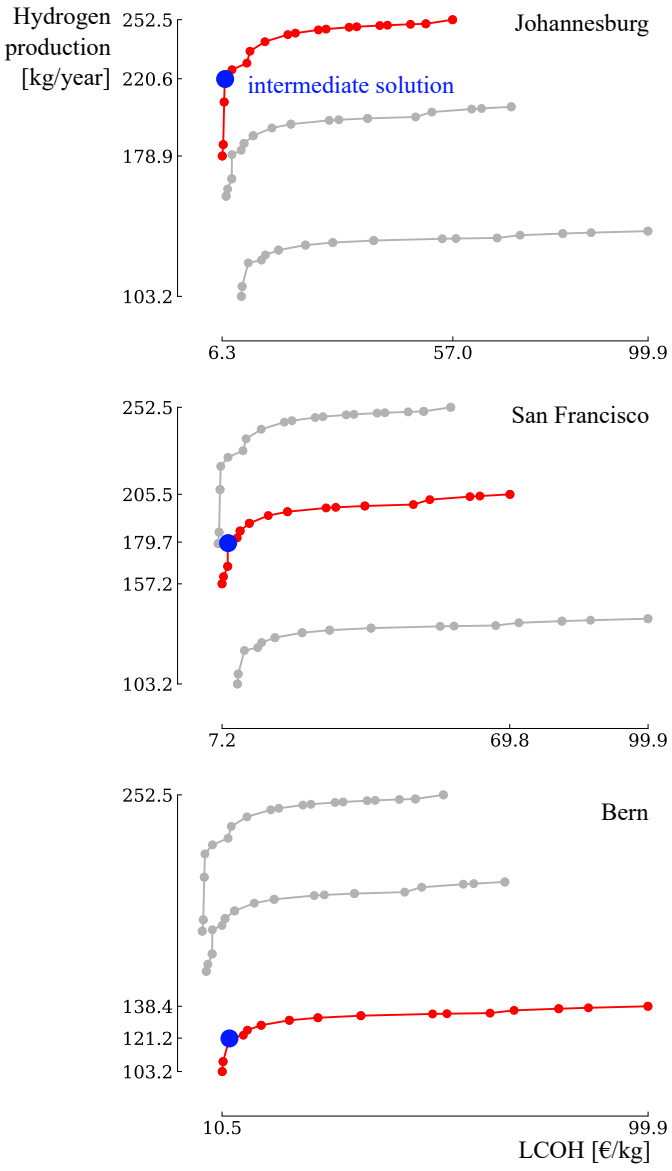

Figure 3: A trade-off exists between maximizing the hydrogen production and minimizing the Levelized Cost Of Hydrogen (LCOH) in each considered location. Next to the 2 extreme designs, an intermediate solution is appointed as well. In Johannesburg, the optimal LCOH and hydrogen production is achieved.

Johannesburg, 64 % in San Francisco and 69 % in Bern (Figure 5). Hence, this result demonstrates the importance of low-interest loan policies and technology

Table 3: For each location, the same electrolyzer stack design leads to a maximum hydrogen production. To acquire the minimum Levelized Cost Of Hydrogen (LCOH), the number of electrolyzers is significantly lower, with slight differences in operating temperature for each location. As a trade-off between both extremes, an intermediate design is presented, which drastically increases the hydrogen production compared to the cost efficient design, at the expense of a slight increase in LCOH.

Location	N_s	N_p	T_elec	LCOH	$\dot{m}_{\mathrm{H_2}}$	$E_\mathrm{elec,year}/E_\mathrm{MPP,year}$
			K	€/kg	kg/year	%
Bern	10	2	331	10.5	103.2	93.5
	12	30	353	99.9	138.4	98.7
	10	3	353	12.1	121.2	97.9
San Francisco	10	2	336	7.2	157.2	95.8
	12	30	353	69.8	205.5	99.3
	10	3	353	8.5	179.7	98.4
Johannesburg	10	2	333	6.3	178.9	88.9
	12	30	353	57.0	252.5	98.4
	10	3	353	6.9	220.6	99.1

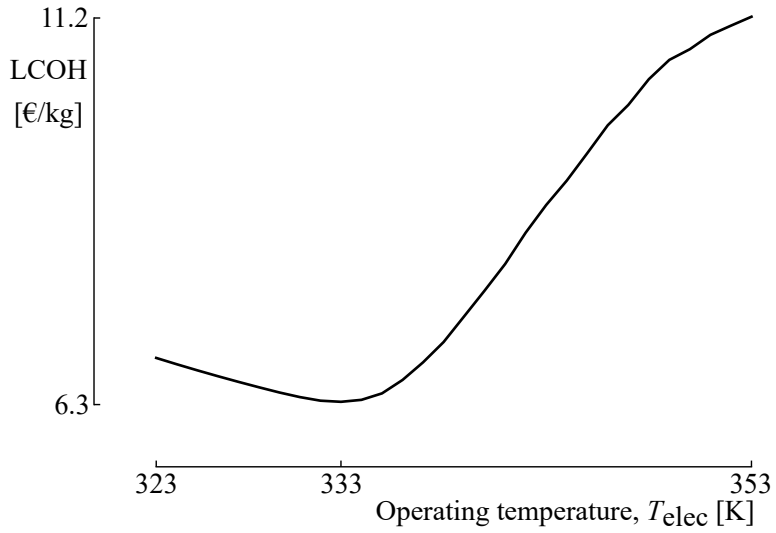

Figure 4: When performing a sensitivity analysis on the operating temperature of the cost-efficient design in Johannesburg, the LCOH can increase up to 78 % when deviating from the optimal operating temperature of 333 K.

de-risking for the economic maturity of PV-electrolyzer systems. Moreover, this result shows the increasing importance of reducing the discount rate in locations with a lower total yearly solar irradiance, since the LCOH reduction effect is the largest in Bern, followed by San Francisco and Johannesburg.

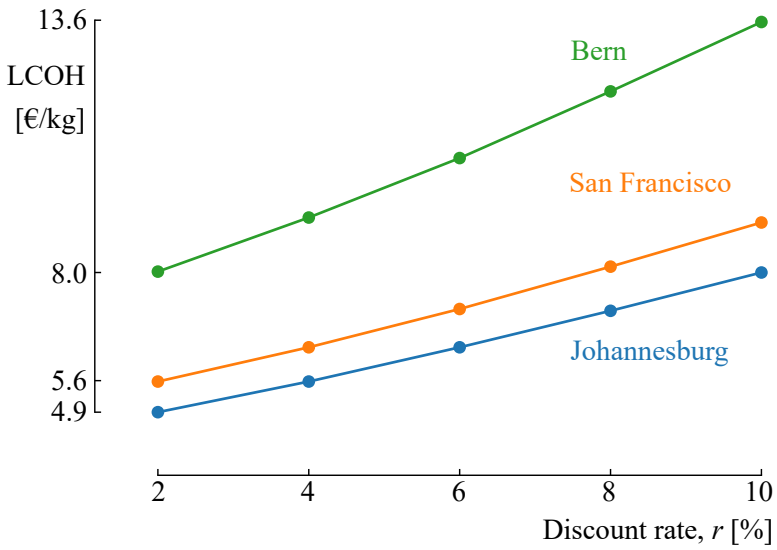

Figure 5: Increasing the discount rate from 2 % to 10 % increases the Levelized Cost Of Hydrogen (LCOH) of the PV-electrolyzer system by 63 % in Johannesburg, 64 % in San Francisco and 69 % in Bern.

3.2. Surrogate-assisted Robust Design Optimization

In this section, the stochastic dimension reduction is performed. Then, the surrogate-assisted RDO results are presented and discussed, followed by the most contributing parameters to the objective variation. To conclude, a sensitivity analysis is performed of the discount rate.

3.2.1. Stochastic dimension reduction

The stochastic dimension reduction is applied for both the hydrogen production and LCOH separately, since the model parameter uncertainties contribute differently to each objective. For the LCOH, most economic parameters, the solar irradiance, membrane area and short-circuit current are the parameters

contributing more than 2 % to the standard deviation in at least one considered design sample (Table 4). The $\mathrm{CAPEX_{PV}}$ is a significant contributor to the LCOH variance in PV-electrolyzer system designs with a relatively small amount of electrolyzers installed. In such a design, the LCOH depends mainly on the cost of installed PV panels, and therefore the LCOH variation depends mainly on the $\mathrm{CAPEX_{PV}}$ variation. When the hydrogen production is selected as an objective, evidently the economic parameters do not contribute to the variation. Instead, the solar irradiance is the most dominant parameter (Table 4).

Respectively, the uncertainty of only 8 and 7 parameters remain significant for the LCOH and hydrogen production. As a result, the total required number of model evaluations is reduced to 330 for 8 stochastic parameters and 240 for 7 parameters, as opposed to 2660 for the full stochastic space. Consequently, the computational cost is reduced by 87.5 % and 90.9 % respectively to achieve statistical moments for each considered objective.

Table 4: The maximum Sobol' index above the threshold for each parameter over the considered design samples are presented. Therefore, these parameters are considered uncertain in the surrogate-assisted Robust Design Optimization (RDO). The CAPEX parameters, discount rate r and solar irradiance G are the most contributing parameters to the LCOH variation in at least one of the considered design samples. For the hydrogen production, the variation is mainly dominated by the solar irradiance G.

LCOH		hydrogen production	
parameter	value, %	parameter	value, %
$\mathrm{CAPEX_{PV}}$	80	G	91
r	51	A_{m}	18
$\mathrm{CAPEX_{elec}}$	40	I_{SC}	12
G	22	T_{elec}	12
$\mathrm{OPEX_{elec}}$	5	t_{m}	6
n_{elec}	4	T_{amb}	5
A_{m}	3	n_{elec}	2
I_{SC}	2		

3.2.2. Surrogate-assisted Robust Design Optimization on the hydrogen production

The surrogate-assisted RDO algorithm is applied to the PV-electrolyzer system, to find a Pareto set of design samples that makes a trade-off between maximizing the mean hydrogen production and minimizing the standard deviation for each considered location (Figure 6). The converged Pareto front is achieved around 80 generations for the considered locations. As the most robust design corresponds to a negligible mean hydrogen production, this design is not considered. Instead, an intermediate design is presented for each location, which achieves a significant drop in standard deviation (from 43 % in Johannesburg up to 56 % in Bern), at the expense of a tolerable decrease in mean hydrogen production (from 23 % in Johannesburg up to 34 % in Bern, Table 5).

Clearly, the effect of a more severe constraint on the limiting current does not imply a reduction of the maximum mean hydrogen production, compared to the predicted deterministic hydrogen production. With 30 electrolyzer strings in parallel, this design is clearly oversized, reaching a limiting current far above the highest current produced by the PV system. Therefore, the energy from the PV system at each hour is transferred to the electrolyzer stack, even if the limiting current is a bit more severe.

When quantifying the contribution of the stochastic input parameters to the standard deviation of the hydrogen production in the intermediate design, the solar irradiance is the dominating parameter (Table 6). Hence, increased accuracy in solar irradiance data and predictions is the most significant action to improve the quality and robustness of the hydrogen production.

3.2.3. Techno-economic surrogate-assisted Robust Design Optimization

Next to the hydrogen production, the surrogate-assisted RDO algorithm is applied for the LCOH. In this approach, no trade-off exists between minimizing the LCOH standard deviation and minimizing the mean LCOH. Hence, the robust design achieves the optimal mean LCOH as well. Moreover, this design consists of the same configuration as the previously found deterministic design

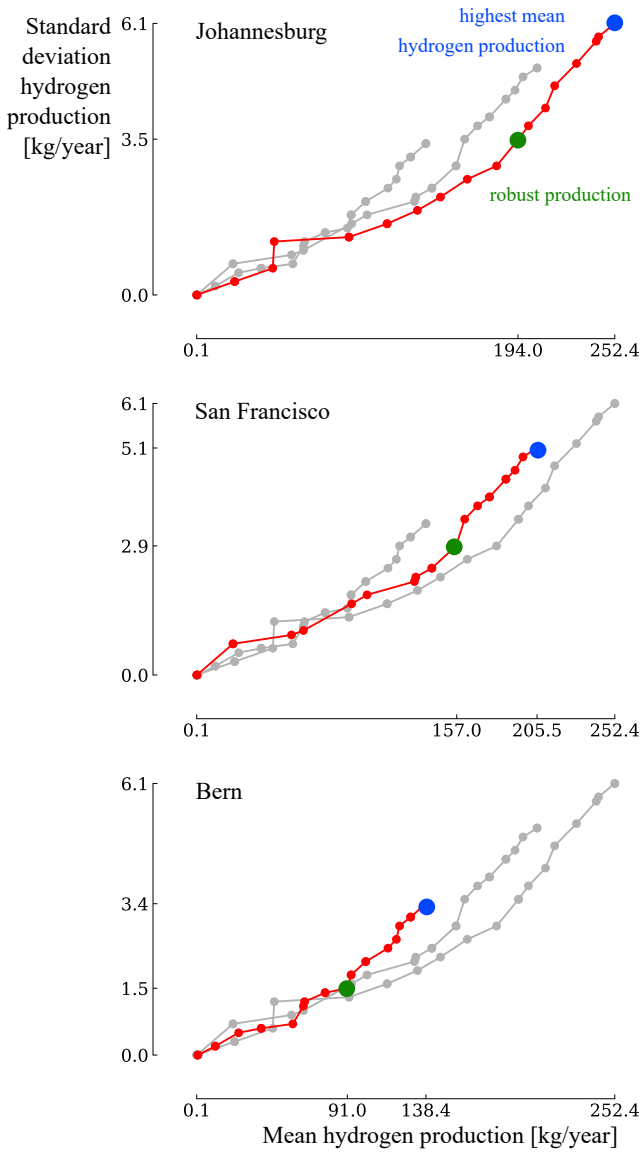

Figure 6: A clear trade-off exists between maximizing the mean hydrogen production and minimizing the standard deviation of the hydrogen production in all locations. The minimum standard deviation is found at a negligible production. Therefore, an intermediate, practical solution is presented as a robust design instead.

leading to the minimum LCOH in each location (Table 3). Clearly, the standard deviation of the LCOH is the lowest for the PV-electrolyzer system installed in

Table 5: For each location, the same electrolyzer stack design leads to a maximum hydrogen production and a minimal Levelized Cost Of Hydrogen (LCOH), with slight differences in the operating temperature for each location. An intermediate design is found, which drastically increases the hydrogen production compared to the cost efficient design, at the expense of a slight increase in LCOH.

Location	N_s	N_p	T_elec	$\sigma_{\dot{m}_{\mathrm{H_2}}}$	$\mu_{\dot{m}_{\mathrm{H_2}}}$
			K	kg/year	kg/year
Bern	11	2	331	1.5	91.0
	30	12	353	3.4	138.4
San Francisco	11	2	349	2.9	157.0
	30	12	353	5.1	205.5
Johannesburg	11	2	351	3.5	194.0
	30	12	353	6.1	252.4

the location with the highest total yearly solar irradiance (i.e. Johannesburg) (Figure 7). An optimal LCOH standard deviation of 0.74€/kg is achieved in Johannesburg, followed by 0.84€/kg in San Francisco and 1.26€/kg in Bern. Therefore, installing PV-electrolyzer systems in locations with high yearly total solar irradiance is not only beneficial for the mean LCOH, but also ensures optimal robustness. Due to the more severe constraint on the limiting current, the mean LCOH for each location is slightly increased compared to the LCOH achieved in the corresponding deterministic design (Table 3). Due to the reduced limiting current, the operating range of the electrolyzer stack is reduced, leading to a decrease in total transferred current from the PV system to the electrolyzer stack over the year, eventually leading to a decreased yearly hydrogen production. The uncertainty on the discount rate and CAPEX parameters dominates the LCOH standard deviation by 91 % (Table 6). Therefore, bulk manufacturing of these systems to reduce the CAPEX variation and more demonstration projects to stabilize the discount rates are the main actions to improve the LCOH robustness. During system operation (i.e. CAPEX and

discount rate fixed), the electrolyzer lifetime and OPEX are the dominating parameters. Therefore, ensuring high-quality maintenance is the main action to ensure the LCOH robustness.

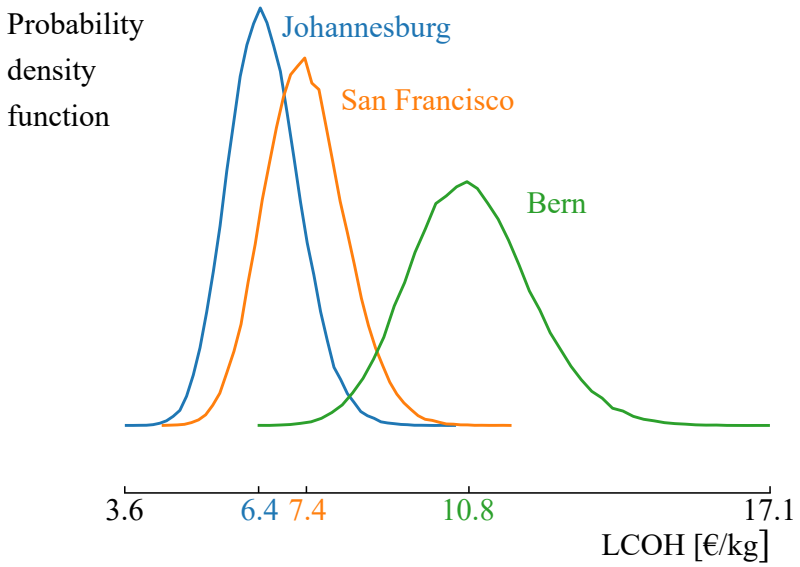

Figure 7: The mean LCOH is optimal in the location with the highest total yearly solar irradiance, Johannesburg. Moreover, the robust design in Johannesburg achieves the lowest standard deviation out of the robust designs in all considered locations.

3.2.4. Sensitivity analysis of the discount rate during system operation

When the PV-electrolyzer system is designed for an optimal LCOH, the variation is mainly dominated by the CAPEX parameters and the discount rate (subsubsection 3.2.3). These parameters can be considered uncertain in the planning stage, but are fixed during system operation. Therefore, to illustrate the effect of the discount rate on the LCOH during system operation under uncertainty, we consider the CAPEX parameters deterministic, while different discrete non-probabilistic scenarios for the discount rate are evaluated. For each location, the robust design is presented for variable discount rates between 2 % and 10 % (Figure 8). As expected, an increasing discount rate escalates the mean LCOH. However, the standard deviation drops for an increasing discount

Table 6: The Sobol' indices are quantified for the robust design for the Levelized Cost Of Hydrogen (LCOH) and hydrogen production. The LCOH variation is dominated by the discount rate r and the CAPEX parameters of the PV-electrolyzer system. The uncertainty on the solar irradiance dominates the variation of the hydrogen production.

LCOH		hydrogen production	
parameter	value, %	parameter	value, %
r	52	G	85
$\mathrm{CAPEX_{PV}}$	23	I_{SC}	4
$\mathrm{CAPEX_{elec}}$	16	A_{m}	3
n_{elec}	5	T_{elec}	3
$\mathrm{OPEX_{elec}}$	3	T_{amb}	2
G	1	t_{m}	2
A_{m}	1		

rate. Moreover, this stabilizing effect increases when considering less optimal locations. Since the effect on the mean LCOH is significantly large compared to the gain in robustness, financing the system at the lowest discount rate remains the most beneficial situation.

4. Conclusion

Directly coupled photovoltaic-electrolyzer systems deliver a viable solution to store solar energy in the form of hydrogen. From a techno-economic perspective, such a system should achieve a minimum levelized cost of hydrogen. A configuration of 2 parallel strings of 10 electrolyzers in series results in a minimum levelized cost of hydrogen ranging between 6.3 €/kg (Johannesburg) and 10.5 €/kg (Bern). Despite the equal number of electrolyzers in each design, the operating temperature is different, ranging between 331 K and 336 K for the different locations. A sensitivity analysis of the discount rate from 10 % to 2 % illustrates that the levelized cost of hydrogen can be decreased by 63 % in the optimal location and 69 % in the least optimal location. Therefore, low-interest loan policies and de-risking of the technology are crucial to improve the

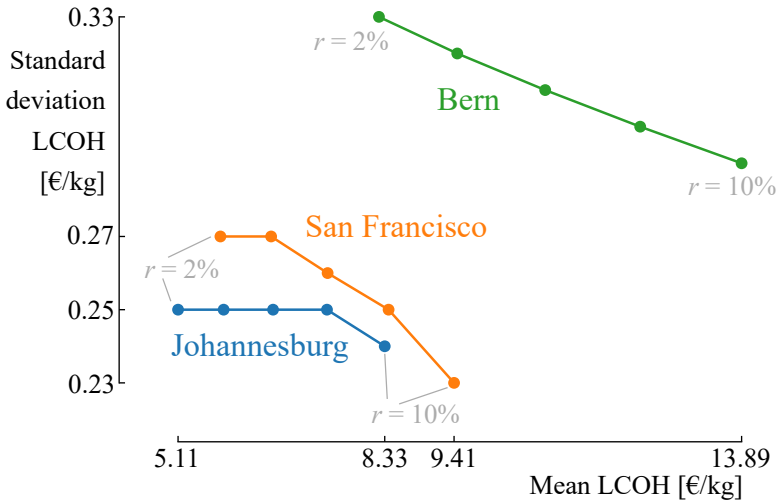

Figure 8: Despite that the discount rate is proportional to the mean LCOH, it reduces the standard deviation and therefore provides a stabilizing effect for the LCOH of the PV-electrolyzer system. The discount rate is varied in steps of 2 %.

economic maturity of the photovoltaic-electrolyzer system, especially in suboptimal climate conditions.

When considering uncertainty on the techno-economic model parameters, a robust design for the hydrogen production is proposed, where a decrease in standard deviation is acquired (from 43 % in Johannesburg up to 56 % in Bern), at the expense of a reduction in mean hydrogen production (from 23 % in Johannesburg up to 34 % in Bern). The solar irradiance is the main contributor to the hydrogen production variation in the robust design, representing 85 % of the total variation. Consequently, increased solar irradiance data accuracy and more accurate predictions are the most significant improvements to increase the hydrogen production quality during real-life system operation.

No trade-off is found between minimizing the mean levelized cost of hydrogen and minimizing the standard deviation. The levelized cost of hydrogen statistical moments are optimal in the location with the highest yearly total solar irradiance (mean levelized cost of hydrogen of 6.4 €/kg at a standard deviation of 0.74 €/kg). Therefore, installing a photovoltaic-electrolyzer system in loca-

tions with a high total yearly solar irradiance is favourable for both the mean and robustness of the levelized cost of hydrogen. The main contributors to the levelized cost of hydrogen variation are the capital expenditure parameters and the discount rate, representing 52 % and 39 % of the total variation, respectively. During system operation, the most significant contributing parameters to the variation are the operational expenditure and lifetime of the electrolyzer stack. Therefore, bulk manufacturing of the technology, promoting more demonstration projects and continuous high-quality maintenance are the most significant actions to improve the levelized cost of hydrogen robustness. An increased discount rate shows to have a stabilizing effect on the levelized cost of hydrogen variation, resulting in a more robust performance. Since the stabilizing effect is small compared to the increase in mean levelized cost of hydrogen, financing the photovoltaic-electrolyzer system with the lowest discount rate is still considered optimal.

Future works will focus on the robust performance of the system when including hydrogen storage, batteries, grid supply and energy demand. Since the large uncertainty on the grid electricity cost, we expect to see that autonomous systems will lead to the most robust solutions.

5. Acknowledgements

This work was supported by Interreg North-West Europe [NWE334] and Fonds de la Recherche Scientifique - FNRS [33856455-5001419F FRIA-B1]

References

[1] E. Kabir, P. Kumar, S. Kumar, A. A. Adelodun, K.-H. Kim, Solar energy: Potential and future prospects, Renewable and Sustainable Energy Reviews 82 (2018) 894–900.

[2] M. Aneke, M. Wang, Energy storage technologies and real life applications–a state of the art review, Applied Energy 179 (2016) 350–377.

[3] A. Khalilnejad, A. Sundararajan, A. I. Sarwat, Optimal design of hybrid wind/photovoltaic electrolyzer for maximum hydrogen production using imperialist competitive algorithm, Journal of Modern Power Systems and Clean Energy 6 (2018) 40–49.

[4] A. Mohammadi, M. Mehrpooya, A comprehensive review on coupling different types of electrolyzer to renewable energy sources, Energy 158 (2018) 632–655.

[5] I. Dincer, C. Acar, Review and evaluation of hydrogen production methods for better sustainability, International journal of hydrogen energy 40 (2015) 11094–11111.

[6] A. Mehmeti, A. Angelis-Dimakis, G. Arampatzis, S. McPhail, S. Ulgiati, Life cycle assessment and water footprint of hydrogen production methods: from conventional to emerging technologies, Environments 5 (2018) 24.

[7] A. Maroufmashat, F. Sayedin, S. S. Khavas, An imperialist competitive algorithm approach for multi-objective optimization of direct coupling photovoltaic-electrolyzer systems, International Journal of Hydrogen Energy 39 (2014) 18743–18757.

[8] R. García-Valverde, N. Espinosa, A. Urbina, Optimized method for photovoltaic-water electrolyser direct coupling, International Journal Of Hydrogen Energy 36 (2011) 10574–10586.

[9] B. A. Pinaud, J. D. Benck, L. C. Seitz, A. J. Forman, Z. Chen, T. G. Deutsch, B. D. James, K. N. Baum, G. N. Baum, S. Ardo, H. Wang, E. Miller, T. F. Jaramillo, Technical and economic feasibility of centralized facilities for solar hydrogen production via photocatalysis and photoelectrochemistry, Energy and Environmental Science 6 (2013) 1983–2002.

[10] F. Sayedin, A. Maroufmashat, S. Sattari, A. Elkamel, M. Fowler, Optimization of Photovoltaic Electrolyzer Hybrid systems; Taking into account

the effect of climate conditions, Energy Conversion and Management 118 (2016) 438–449.

[11] B. Zakeri, S. Syri, Electrical energy storage systems: A comparative life cycle cost analysis, Renewable and sustainable energy reviews 42 (2015) 569–596.

[12] A. Al-Karaghouli, L. L. Kazmerski, Energy consumption and water production cost of conventional and renewable-energy-powered desalination processes, Renewable and Sustainable Energy Reviews 24 (2013) 343–356.

[13] B. Olateju, A. Kumar, A techno-economic assessment of hydrogen production from hydropower in Western Canada for the upgrading of bitumen from oil sands, Energy 115 (2016) 604–614.

[14] B. Sudret, Polynomial chaos expansions and stochastic finite-element methods, 2003, 2014.

[15] T. Chatterjee, S. Chakraborty, R. Chowdhury, A Critical Review of Surrogate Assisted Robust Design Optimization, Archives of Computational Methods in Engineering (2017) 1–30.

[16] S. Abraham, M. Raisee, G. Ghorbaniasl, F. Contino, C. Lacor, A robust and efficient stepwise regression method for building sparse polynomial chaos expansions, Journal of Computational Physics 332 (2017) 461–474.

[17] G. Taguchi, Taguchi on robust technology development. bringing quality engineering upstream, 1993.

[18] A. L. Soyster, Convex programming with set-inclusive constraints and applications to inexact linear programming, Operations research 21 (1973) 1154–1157.

[19] D. Bertsimas, M. Sim, The price of robustness, Operations research 52 (2004) 35–53.

[20] E. Kuznetsova, C. Ruiz, Y.-F. Li, E. Zio, Analysis of robust optimization for decentralized microgrid energy management under uncertainty, International Journal of Electrical Power & Energy Systems 64 (2015) 815–832.

[21] A. Parisio, C. Del Vecchio, A. Vaccaro, A robust optimization approach to energy hub management, International Journal of Electrical Power & Energy Systems 42 (2012) 98–104.

[22] D. E. Majewski, M. Wirtz, M. Lampe, A. Bardow, Robust multi-objective optimization for sustainable design of distributed energy supply systems, Computers & Chemical Engineering 102 (2017) 26–39.

[23] K. Akbari, M. M. Nasiri, F. Jolai, S. F. Ghaderi, Optimal investment and unit sizing of distributed energy systems under uncertainty: A robust optimization approach, Energy and Buildings 85 (2014) 275–286.

[24] MSX-60 and MSX-64 Photovoltaic Modules, Solarex, 1997.

[25] F. M. González-Longatt, Model of Photovoltaic Module in Matlab, in: 2DO Congreso Iberoamericano de estudiantes de ingeniería eléctrica, electrónica y computación (II CIBELEC 2005), 2005, pp. 1–5.

[26] D. Bonkoungou, Z. Koalaga, D. Njomo, Modelling and simulation of photovoltaic module considering single-diode equivalent circuit model in matlab, International Journal of Emerging Technology and Advanced Engineering 3 (2013) 493–502.

[27] Q. Kou, S. A. Klein, W. A. Beckman, A method for estimating the long-term performance of direct-coupled PV pumping systems, Solar Energy 64 (1998) 33–40.

[28] A. Buttler, H. Spliethoff, Current status of water electrolysis for energy storage, grid balancing and sector coupling via power-to-gas and power-to-liquids: A review, Renewable and Sustainable Energy Reviews 82 (2018) 2440–2454.

[29] R. García-Valverde, N. Espinosa, A. Urbina, Simple PEM water electrolyser model and experimental validation, International Journal of Hydrogen Energy 37 (2012) 1927–1938.

[30] R. García-Valverde, C. Miguel, R. Martínez-Béjar, A. Urbina, Optimized photovoltaic generator-water electrolyser coupling through a controlled DC-DC converter, International Journal of Hydrogen Energy 33 (2008) 5352–5362.

[31] B. Paul, Direct-coupling of the photovoltaic array and PEM electrolyser in solar-hydrogen systems for remote area power supply, Ph.D. thesis, RMIT University, 2009.

[32] Meteotest, Handbook part II: Theory, Global Meteorological Database Version 7. Software and Data for Engineers, Planers and Education (2017).

[33] A. Tugirumubano, L. K. Kwac, M. S. Lee, J. H. Lee, J. J. Lee, S. A. Jeon, H. N. Jeong, H. G. Kim, Analysis of the parametric effect on the performance of a polymer electrolyte membrane electrolyzer, International Journal of Mechanical Engineering and Robotics Research 6 (2017) 1–5.

[34] A. H. Fathima, K. Palanisamy, Optimization in microgrids with hybrid energy systems - A review, Renewable and Sustainable Energy Reviews 45 (2015) 431–446.

[35] K. Deb, A. Pratap, S. Agarwal, T. Meyarivan, A fast and elitist multiobjective genetic algorithm: NSGA-II, IEEE Transactions on Evolutionary Computation 6 (2002) 182–197.

[36] P. Tsirikoglou, S. , F. Contino, Ö. Bağci, J. Vierendeels, G. Ghorbaniasl, Comparison of metaheuristics algorithms on robust design optimization of a plain-fin-tube heat exchanger, in: 18th AIAA/ISSMO Multidisciplinary Analysis and Optimization Conference, 2017, p. 3827.

[37] M. Stein, Large sample properties of simulations using latin hypercube sampling, Technometrics 29 (1987) 143–151.

[38] K. Deb, R. B. Agrawal, Simulated Binary Crossover for Continuous Search Space, Complex Systems 9 (1995) 115–148.

[39] K. Deb, S. Agrawal, A niched-penalty approach for constraint handling in genetic algorithms, in: Artificial Neural Nets and Genetic Algorithms, Springer, 1999, pp. 235–243.

[40] G. Mavromatidis, K. Orehounig, J. Carmeliet, A review of uncertainty characterisation approaches for the optimal design of distributed energy systems, Renewable and Sustainable Energy Reviews 88 (2018) 258–277.

[41] L. Reichenberg, F. Hedenus, M. Odenberger, F. Johnsson, The marginal system LCOE of variable renewables Evaluating high penetration levels of wind and solar in Europe, Energy 152 (2018) 914–924.

[42] K. Branker, M. J. Pathak, J. M. Pearce, A review of solar photovoltaic levelized cost of electricity, Renewable and Sustainable Energy Reviews 15 (2011) 4470–4482.

[43] K. Rajeshwar, R. D. McConnell, S. Licht, Solar Hydrogen Generation: Toward a Renewable Energy Future, Springer, 2008.

[44] C. A. Rodriguez, M. A. Modestino, D. Psaltis, C. Moser, Design and cost considerations for practical solar-hydrogen generators, Energy Environ. Sci. 7 (2014) 3828–3835.

[45] F. Segura, V. Bartolucci, J. M. Andújar, Hardware/software data acquisition system for real time cell temperature monitoring in air-cooled polymer electrolyte fuel cells, Sensors (Switzerland) 17 (2017) 1600.

[46] Y. He, M. Razi, C. Forestiere, L. Dal Negro, R. M. Kirby, Uncertainty quantification guided robust design for nanoparticles' morphology, Computer Methods in Applied Mechanics and Engineering 336 (2018) 578–593.

[47] P. Turati, N. Pedroni, E. Zio, Simulation-based exploration of high-dimensional system models for identifying unexpected events, Reliability Engineering and System Safety 165 (2017) 317–330.

[48] F. Sayedin, A. Maroufmashat, R. Roshandel, S. S. Khavas, Optimal design and operation of a photovoltaic-electrolyser system using particle swarm optimisation, International Journal of Sustainable Energy 35 (2014) 566–582.